# EKF-Enhanced Feedback Linearization with Online Actuator Gain Identification for a Dual-Axis Bicopter Platform

Alexander F. Vasquez[a],

[a] *Pontificia Universidad Católica del Perú, Lima, Perú*

**Abstract**

This paper presents a nonlinear control framework for a dual-axis bicopter platform that combines exact input–output feedback linearization with an Extended Kalman Filter (EKF) for state estimation and online actuator gain identification. This dual estimation mechanism enables the controller to compensate for modeling errors and actuator variations in real time. The results demonstrate that, while parameter uncertainty significantly degrades performance, the integration of EKF-based identification restores nominal tracking accuracy and enhances robustness against noise. Overall, the presented methodology provides an effective and reliable solution for nonlinear aerial platforms subject to uncertainty and sensor disturbances.

*Keywords:* Feedback linearization, Extended Kalman filter, Nonlinear control, Parameter identification, UAV dynamics, Bicopter

## 1. Introduction

The importance of unmanned aerial vehicles (UAVs) has grown significantly in recent years due to their wide range of applications in fields such as mining, precision agriculture, inspection, and surveillance. These systems often operate in uncertain and dynamically changing environments, where external disturbances, sensor noise, and parametric uncertainty are unavoidable. Moreover, because UAV platforms exhibit inherently unstable, nonlinear, and multivariable dynamics [1], achieving reliable control requires a solid understanding of advanced control theory. In addition, most UAVs are underactuated systems, which limits the applicability of classical control strategies designed for fully actuated platforms [2]. These challenges are further compounded by model uncertainties, actuator faults, strong subsystem coupling, measurement noise, and external disturbances, all of which significantly affect performance and motivate the development of robust and adaptive control methodologies [3].

To support the study and validation of such control methods, laboratory platforms like the Quanser AERO 2-DOF system have become widely used. This setup consists of a bicopter-like mechanism with two rotors rigidly mounted on a base, enabling rotation about the pitch and yaw axes. Its mechanical simplicity, combined with experimentally validated parameters, makes it an ideal testbed for developing and evaluating nonlinear control algorithms. A detailed dynamic model of this type of pitch–yaw mechanism has been previously explored in [4, 5, 6, 7], and a concise description of the AERO system is provided in the manufacturer's documentation [8], which serves as a foundation for modeling in this work.

Several studies have addressed the control of bicopter systems with dynamic coupling and uncertain parameters. For example, adaptive nonlinear control approaches have been employed to compensate for unknown dynamics [9], while adaptive backstepping strategies in pure feedback form have been proposed to avoid explicit inversion of the input map [10]. These contributions highlight the relevance of combining nonlinear control laws with estimation techniques to improve robustness under model uncertainty and actuator coupling.

In this work, the pitch and yaw states of the platform—typically obtained through IMU sensors and encoder measurements—are considered to be

*Email address:* alexanderf.vasquez@pucp.edu.pe (Alexander F. Vasquez )

affected by measurement noise. This motivates the use of an Extended Kalman Filter (EKF) as an observer to provide accurate state estimation. Furthermore, since actuator thrust gains are often obtained through empirical calibration and may vary during operation, the EKF is also employed to perform online parameter identification. This dual estimation capability is essential to ensure that the feedback-linearizing controller receives consistent state and parameter information despite noise and uncertainty.

The remainder of this paper is organized as follows. Section 2 presents the mathematical modeling of the pitch–yaw system, including actuator coupling and nonlinear dynamics. Section 3 describes the proposed control methodology, combining input–output feedback linearization, state estimation, and online parameter identification. Section 4 provides simulation results evaluating performance under parameter uncertainty and measurement noise. Finally, conclusions and future research directions are discussed in Section 5.

## 2. Mathematical System Modeling

This section develops the mathematical model of the dual–axis system (pitch–yaw) under consideration. The model is derived from the free–body diagram (FBD), energy expressions, and actuator characteristics of the system. The resulting representation is expressed in a nonlinear state–space form suitable for analysis and control design.

### *2.1. Dynamic Description of the Pitch–Yaw Mechanism*

The system consists of a rigid body capable of rotating about two orthogonal axes: pitch $\theta$ and yaw $\psi$. Each axis is actuated by electric motors that generate thrust forces, producing control torques. Additionally, gravitational torque and mechanical damping are present in the pitch axis.

From the free-body diagram (Fig. 1), the forces acting on the system include:

- $F_{pp}, F_{py}$: thrust forces generated by the pitch motor due to pitch and yaw voltages.

- $F_{yp}, F_{yy}$: thrust forces generated by the yaw motor due to yaw and pitch voltages.

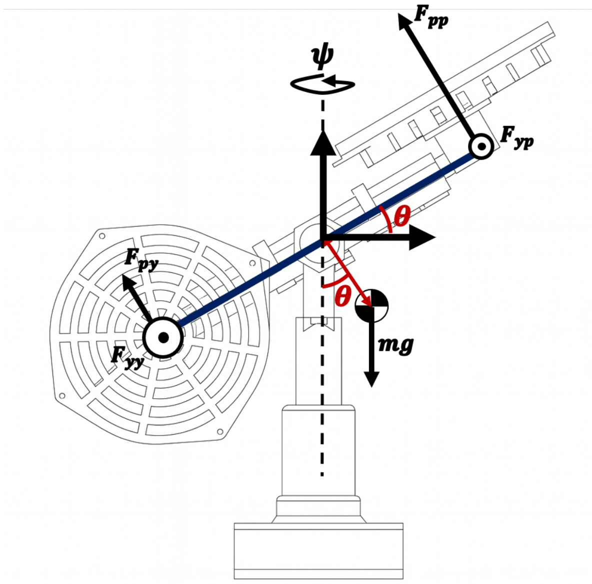


Figure 1: Free Body Diagram of the system

The gravitational component $mg$ influences only the pitch axis. Mechanical damping torques are given by:

$$T_{dp} = -D_{vp}\dot{\theta}, \qquad T_{dy} = -D_{vy}\dot{\psi}.$$

The physical system is subject to the following mechanical constraints:

$$-60^\circ \leq \theta \leq 60^\circ, \qquad V_p,\, V_y \in [-24\text{ V},\, 24\text{ V}].$$

### *2.2. Actuator Model and Cross–Coupling Effects*

The pitch and yaw torques are generated according to:

$$T_p = T_{pp} + T_{py}, \tag{1}$$
$$T_y = T_{yy} + T_{yp}. \tag{2}$$

The voltage–to–thrust relationships are modeled as:

$$T_p = k_{pp}V_p + k_{py}V_y, \tag{3}$$
$$T_y = k_{yy}V_y + k_{yp}V_p. \tag{4}$$

The coefficients $k_{pp}$ and $k_{yy}$ correspond to the direct thrust gains, while $k_{py}$ and $k_{yp}$ model cross–coupling effects between pitch and yaw actuation.

All physical parameters are summarized in Table 1.

### 2.3. Kinetic and Potential Energies

Given the rotational inertias $I_p$ and $I_y$, and the distance from the pivot to the center of mass $l_{cm}$, the total kinetic energy of the system is:

$$K = \frac{1}{2}I_p\dot{\theta}^2+\frac{1}{2}I_y\dot{\psi}^2+\frac{1}{2}l_{cm}^2 m\left(\dot{\theta}^2+\dot{\psi}^2\sin^2\theta\right). \quad (5)$$

The gravitational potential energy is:

$$V = -mgl_{cm}\cos\theta. \quad (6)$$

Using Lagrange's equations

$$\frac{d}{dt}\left(\frac{\partial K}{\partial \dot{q}}\right) - \frac{\partial K}{\partial q} + \frac{\partial V}{\partial q} = \tau_q,$$

with generalized coordinates $q = [\theta,\ \psi]^T$, the nonlinear equations of motion are obtained.

### 2.4. Nonlinear Dynamic Model

The nonlinear dynamics of the pitch–yaw system are given by the following differential equations:

$$\ddot{\theta} = \frac{k_{pp}V_p+k_{py}V_y-D_{vp}\dot{\theta}+ml_{cm}^2\dot{\psi}^2\sin(\theta)\cos(\theta)-mgl_{cm}\sin(\theta)}{I_p+ml_{cm}^2} \quad (7)$$

$$\ddot{\psi} = \frac{k_{yy}V_y+k_{yp}V_p-D_{vy}\dot{\psi}-2ml_{cm}^2\dot{\psi}\dot{\theta}\sin(\theta)\cos(\theta)}{I_y+ml_{cm}^2\sin^2(\theta)} \quad (8)$$

Considering the state variables

$$x_1 = \theta, \quad x_2 = \dot{\theta}, \quad x_3 = \psi, \quad x_4 = \dot{\psi},$$

the state–space model can be rewritten in strict–feedback form as

$$x = \begin{bmatrix} x_1 \\ x_2 \\ x_3 \\ x_4 \end{bmatrix}, \qquad u = \begin{bmatrix} V_p \\ V_y \end{bmatrix}, \qquad \dot{x} = f(x) + g(x)u,$$

$$f(x) = \begin{bmatrix} x_2 \\ A_1(x) \\ x_4 \\ A_2(x) \end{bmatrix} \quad (9)$$

$$g(x) = \begin{bmatrix} \mathbf{0}_{1\times 2} \\ B_1 \\ \mathbf{0}_{1\times 2} \\ B_2 \end{bmatrix} \quad (10)$$

where the nonlinear drift terms are

$$A_1(x) = \frac{-D_{vp}x_2+ml_{cm}^2x_4^2\sin(x_1)\cos(x_1)-mgl_{cm}\sin(x_1)}{I_p+ml_{cm}^2} \quad (11)$$

$$A_2(x) = \frac{-D_{vy}x_4 - 2ml_{cm}^2x_4x_2\sin(x_1)\cos(x_1)}{I_y+ml_{cm}^2\sin^2(x_1)}. \quad (12)$$

and the input vector fields are

$$B_1(x) = \begin{bmatrix} \frac{\kappa_{pp}}{I_p+m\,l_c^2} & \frac{\kappa_{py}}{I_p+m\,l_c^2} \end{bmatrix} \quad (13)$$

$$B_2(x) = \begin{bmatrix} \frac{\kappa_{yp}}{I_y+m\,l_cm^2\sin^2(x_h)} & \frac{\kappa_{yy}}{I_y+m\,l_cm^2\sin^2(x_h)} \end{bmatrix} \quad (14)$$

## 3. Control Design Methodology

This section presents the complete control methodology for the bicopter pitch–yaw platform. The objective is to guarantee accurate trajectory tracking in both axes despite parametric uncertainty and sensor noise. The proposed strategy combines three components: (i) exact input–output feedback linearization, (ii) an Extended Kalman Filter (EKF)–based observer for state reconstruction, and (iii) online identification of thrust gains required for the linearizing control law.

### 3.1. Strict–Feedback Form and Zero Dynamics Analysis

From the nonlinear model derived in Section 2, and using the outputs

$$y_1 = \theta = x_1, \qquad y_2 = \psi = x_3,$$

the system admits the strict–feedback representation:

$$\dot{y}_1 = x_2, \qquad \dot{y}_2 = x_4,$$

and

$$\dot{x}_2 = A_1(x) + B_1(x)u, \qquad \dot{x}_4 = A_2(x) + B_2(x)u, \quad (15)$$

Since $I_p + ml_{cm}^2 > 0$ and $I_y + ml_{cm}^2\sin^2(\theta) > 0$ for all admissible angles, the decoupling matrix

$$B(x) = \begin{bmatrix} B_1(x) \\ B_2(x) \end{bmatrix}$$

Table 1: Physical parameters of the pitch–yaw system adapted from [7]

| Parameter | Symbol | Typical Value |
|---|---|---|
| Moment of inertia in pitch | $I_p$ | $0.0219\,\mathrm{kgm}^2$ |
| Moment of inertia in yaw | $I_y$ | $0.0219\,\mathrm{kgm}^2$ |
| Distance from fixed frame to COM | $l_{cm}$ | $2.42\,\mathrm{mm}$ |
| Mass | $m$ | $1.15\,\mathrm{kg}$ |
| Thrust and voltage gain in pitch | $k_{pp}$ | $0.01144\,\mathrm{Nm/V}$ |
| Thrust and voltage gain in yaw | $k_{yy}$ | $0.01144\,\mathrm{Nm/V}$ |
| Cross gain (yaw thrust vs pitch voltage) | $k_{yp}$ | $0.00950\,\mathrm{Nm/V}$ |
| Cross gain (pitch thrust vs yaw voltage) | $k_{py}$ | $0.00980\,\mathrm{Nm/V}$ |
| Pitch damping coefficient | $D_{vp}$ | $0.0072\,\mathrm{Nms/rad}$ |
| Yaw damping coefficient | $D_{vy}$ | $0.0085\,\mathrm{Nms/rad}$ |

never vanishes. Hence, the system is feedback linearizable and the internal (zero) dynamics are identically zero, i.e., the system has *no internal dynamics*. This property allows the design of an exact input–output linearizing control law.

### 3.2. Input–Output Feedback Linearization

Differentiating the outputs twice yields:

$$\ddot{y}_1 = A_1(x) + B_1(x)u, \tag{16}$$

$$\ddot{y}_2 = A_2(x) + B_2(x)u. \tag{17}$$

Grouping them in vector form:

$$\begin{bmatrix} \ddot{y}_1 \\ \ddot{y}_2 \end{bmatrix} = \begin{bmatrix} A_1 \\ A_2 \end{bmatrix} + \begin{bmatrix} B_1 \\ B_2 \end{bmatrix} u,$$

we introduce the virtual control input $v = [v_1\ v_2]^T$ and define:

$$u = B(x)^{-1}\big(v - A(x)\big), \tag{18}$$

so that the input–output dynamics become the fully decoupled linear system:

$$\ddot{y}_1 = v_1, \qquad \ddot{y}_2 = v_2.$$

### 3.3. Trajectory Tracking Control Law

Let the desired trajectories be $\theta_d(t)$ and $\psi_d(t)$, satisfying their respective smoothness requirements. Define the tracking errors:

$$e_\theta = y_1 - \theta_d(t), \quad \dot{e}_\theta = \dot{y}_1 - \dot{\theta}_d(t),$$

and similarly for $\psi$. Choosing the second–order linear stabilizing law:

$$v_1 = \ddot{\theta}_d(t) - k_1\dot{e}_\theta - k_2 e_\theta, \tag{19}$$

$$v_2 = \ddot{\psi}_d(t) - k_3\dot{e}_\psi - k_4 e_\psi, \tag{20}$$

ensures exponential convergence of both tracking errors.

Substituting $v_1, v_2$ into (18) yields the complete nonlinear control law:

$$u = B(x)^{-1}\left(\begin{bmatrix} \ddot{\theta}_d - k_1\dot{e}_\theta - k_2 e_\theta \\ \ddot{\psi}_d - k_3\dot{e}_\psi - k_4 e_\psi \end{bmatrix} - \begin{bmatrix} A_1 \\ A_2 \end{bmatrix}\right).$$

### 3.4. Observer and Online Parameter Identification

Accurate feedback linearization requires the knowledge of all states and of the input gains $(k_{pp}, k_{py}, k_{yp}, k_{yy})$, which are uncertain and subject to modeling errors.

To overcome this difficulty, an Extended Kalman Filter (EKF) is used to simultaneously estimate:

$$x = [\theta,\ \dot{\theta},\ \psi,\ \dot{\psi}]^T, \qquad \varphi = [k_{pp},\ k_{yy}]^T.$$

The augmented state vector is:

$$X_e = \begin{bmatrix} x \\ \varphi \end{bmatrix} \in \mathbb{R}^8.$$

Its dynamics follow:

$$\dot{X}_e = \begin{bmatrix} f(x) + g(x,\varphi)u \\ 0 \end{bmatrix} + \begin{bmatrix} w_x \\ w_\varphi \end{bmatrix},$$

where $w_x, w_\varphi$ are process noise terms. Linearization about the current estimate yields the EKF matrices:

$$A(t) = \frac{\partial(f(x) + g(x,\hat{\varphi})u)}{\partial X_e}\Big|_{(\hat{x},\hat{\varphi})}, \qquad C(t) = \frac{\partial(y)}{\partial X_e},$$

and the Kalman gain:

$$L(t) = P(t)C(t)^T R^{-1},$$

where $R$ is the sensor noise covariance.

The EKF innovation is defined as

$$\tilde{y}(t) = y(t) - h(\hat{x}(t)), \tag{21}$$

where $h(\hat{x}(t))$ is the measurement model.

$$h(\hat{x}(t)) = \begin{bmatrix} \hat{x_1}(t) \\ \hat{x_3}(t) \end{bmatrix}, \tag{22}$$

The time evolution of the estimated augmented state is

$$\dot{\hat{x}}(t) = f\big(\hat{x}(t), \hat{\varphi}(t), u(t)\big) + L(t)\,\tilde{y}(t), \tag{23}$$

where $L(t)$ is the Kalman gain.

The covariance matrix satisfies the Riccati differential equation

$$\dot{P}(t) = A(t)P(t) + P(t)A(t)^T + Q - P(t)C(t)^T R^{-1} C(t)P(t) \tag{24}$$

where $Q$ and $R$ are the process and measurement noise covariance matrices, respectively.

### *3.5. Complete Control Architecture*

The overall control structure, figure 2, is composed of the following interconnected blocks:

- The nonlinear plant (bicopter pitch–yaw dynamics).
- The EKF–based observer/identifier producing $\hat{x}$ and $\hat{\varphi}$.
- The input–output linearization block computing $A(x)$ and $B(x)$.
- The linear controller generating the virtual inputs $v_1, v_2$.
- The linearizing law computing the physical control inputs $u = [V_p, V_y]^T$.

This structure ensures noise attenuation, online parameter adaptation, and exact input–output behavior.

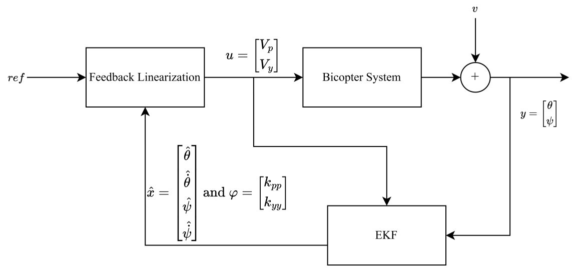


Figure 2: Complete Control Architecture

## 4. Simulation Results

This section presents numerical simulations designed to evaluate the performance of the proposed feedback–linearization controller with state estimation and parameter identification. The assessment is structured into three scenarios: (i) parametric uncertainty without identification, (ii) adaptive parameter identification via an EKF, and (iii) robustness under measurement noise.

From (18), the gains used were:

$$k_1 = 1.7, \qquad k_2 = 7, \qquad k_3 = 1.7, \qquad k_4 = 7.$$

For the EKF, the weighting matrices used in the simulations were:

$$Q = I_6,$$
$$R = 4{,}000{,}000\, I_2.$$

### *4.1. Case 1: Parametric Uncertainty Without Identification*

In this scenario, the controller operates with fixed incorrect actuator gains, $\tilde{k}_{pp} \neq k_{pp}$ and $\tilde{k}_{yy} \neq k_{yy}$. The observer estimates only the system states and does not attempt to identify the uncertain parameters.

Figure 3 illustrates a clear degradation in tracking accuracy. These results confirm the inherent sensitivity of the feedback–linearized system to parameter variations when no adaptation mechanism is incorporated.

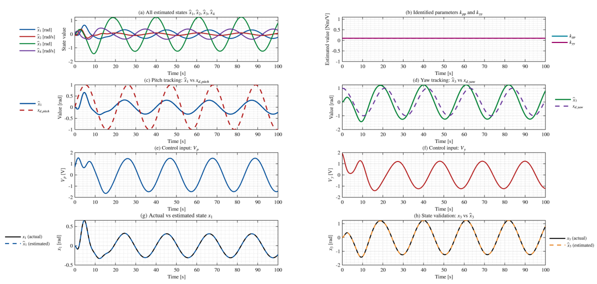

Figure 3: Controller designed assuming $k_{pp} = k_{yy} = 0.099$. (a) Bounded estimated states. (b) Constant actuator gains. (c) Degraded pitch tracking due to parameter mismatch. (d) Yaw tracking, still acceptable despite uncertainties. (e) Pitch control voltage. (f) Yaw control voltage. (g) Estimated pitch state $x_1$. (h) Estimated pitch state $x_2$.

### 4.2. Case 2: Full Controller with EKF Parameter Identification

In this case, the extended Kalman filter estimates both the system states and the uncertain actuator gains, $\hat{k}_{pp}(t)$ and $\hat{k}_{yy}(t)$. Figure 4 shows that the EKF rapidly converges toward the true parameter values, restoring nominal tracking performance.

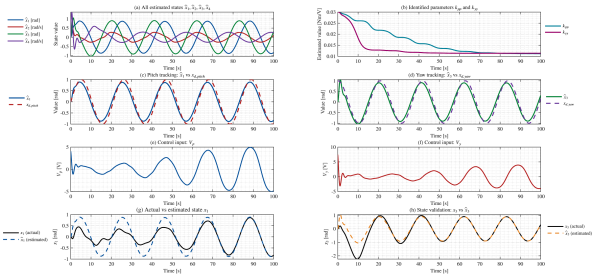

Figure 4: Controller with real-time estimation of $k_{pp}$ and $k_{yy}$. (a) Bounded estimated states. (b) Convergence of the actuator gains. (c) Improved pitch tracking. (d) Improved yaw tracking. (e) Pitch control voltage. (f) Yaw control voltage. (g) Estimated pitch state $x_1$. (h) Estimated pitch state $x_2$.

### 4.3. Case 3: Robustness Under Measurement Noise

In the final evaluation, Gaussian noise is added to the angular measurements $\theta$ and $\psi$. Only the complete control architecture (feedback linearization + observer + EKF).

Figure 5 demonstrates that the EKF effectively attenuates sensor noise and preserves accurate parameter estimation, enabling the controller to maintain reliable tracking performance.

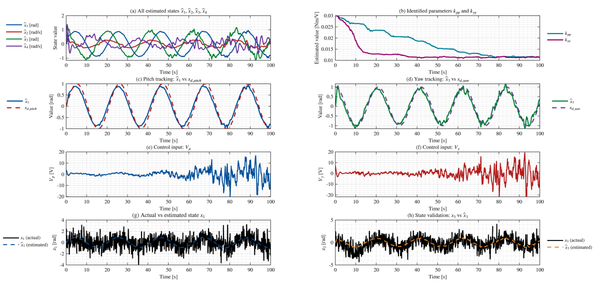

Figure 5: Controller with real-time estimation of $k_{pp}$ and $k_{yy}$ under Gaussian noise of standard deviation 0.01 (approximately 31.6% of the reference amplitude). (a) Bounded estimated states. (b) Convergence of the actuator gains. (c) Robust pitch tracking. (d) Robust yaw tracking. (e) Pitch control voltage. (f) Noisy yaw control voltage. (g) Noisy pitch measurement and estimated $x_1$. (h) Estimated pitch state $x_2$.

### 4.4. Performance Analysis and Comparison

The results across the three scenarios allow for a clear comparative evaluation of the proposed control architecture:

- **State estimation:** In all scenarios, the observer successfully estimated the system states, demonstrating the effectiveness of the state–estimation layer regardless of parameter conditions or noise.
- **Effect of parameter uncertainty:** Scenario 1 revealed that even slight deviations in actuator gains significantly impair tracking performance. This sensitivity is consistent with the structure of feedback linearization, which depends critically on accurate model parameters.
- **Benefits of adaptive estimation:** In Scenario 2, the EKF compensated for the parameter mismatch by driving the estimates toward their true values, thereby restoring nominal tracking behavior. This confirms that online identification is essential for maintaining performance under uncertain conditions.
- **Robustness to measurement noise:** Scenario 3 demonstrated the superior robustness of the full control architecture. Despite substantial measurement noise, the EKF effectively filtered the signals and maintained accurate parameter estimates, enabling reliable tracking.

Overall, the comparison highlights that *state estimation alone is insufficient under parameter uncertainty*, whereas the integration of EKF-based parameter identification significantly enhances both performance and robustness.

## 5. Conclusions and Future Work

This work presented a nonlinear control framework combining feedback linearization, state estimation, and real-time parameter identification through an extended Kalman filter. The simulation results confirm that the proposed strategy achieves accurate tracking under nominal conditions and maintains satisfactory performance in the presence of parameter uncertainties and measurement noise.

The comparative analysis demonstrated that model inaccuracies severely degrade tracking when parameters are fixed, highlighting the need for adaptive mechanisms. Incorporating EKF-based parameter estimation successfully mitigates this limitation by ensuring convergence to the true actuator gains while simultaneously filtering noisy measurements. As a result, the overall architecture exhibits strong robustness and reliability.

Future research will focus on developing adaptive or learning-based controllers capable of generating smoother control inputs, reducing chattering effects observed in some scenarios. Additionally, experimental implementation on a physical test platform will be pursued to validate the proposed approach under real-world operating conditions.

## References


[1] Y. Ding, H. Gao, M. Chen, Modeling and control of quadrotor uavs: Challenges and opportunities, Sensors 25 (4) (2025) 1007. doi:10.3390/s25041007.
URL https://www.mdpi.com/1424-8220/25/4/1007

[2] N. H. Nguyen, S. K. Hong, H. H. Choi, Control strategies for underactuated quadrotor uavs: A review, Annual Reviews in Control 46 (2018) 82–99. doi:10.1016/j.arcontrol.2018.07.003.
URL https://www.sciencedirect.com/science/article/abs/pii/S1367578818300932

[3] M. Benabid, A. Benallegue, O. Azouaoui, A survey of control methods for quadrotor uav, Preprint available on ResearchGate, accessed: 2024-12-01 (2022).
URL https://www.researchgate.net/publication/365296847_A_Survey_of_Control_Methods_for_Quadrotor_UAV

[4] M. Dyvik, D. E. Fjereide, D. Rotondo, Modeling and identification of the quanser aero using a detailed description of friction and centripetal forces, in: Proceedings of the 64th Scandinavian Conference on Simulation and Modeling (SIMS 2023), Linköping University Electronic Press, 2023, pp. 115–122. doi:10.3384/ecp200032.
URL https://ecp.ep.liu.se/index.php/sims/article/view/773/678

[5] R. Fellag, M. Belhocine, Third order super twisting based robust tracking of 2-dof helicopter with state estimation, in: Proceedings of the 21st International Conference on Informatics in Control, Automation and Robotics (ICINCO 2024), SciTePress, 2024, pp. 480–485. doi:10.5220/0013059700003822.
URL https://www.scitepress.org/Papers/2024/130597/130597.pdf

[6] E. Segerstrom, M. Podlaski, A. Khare, L. Vanfretti, Parameter estimation and model validation of quanser aero using modelica and rapid, Journal of Instrumentation and ControlSpecial Issue on UAV / Laboratory Systems (2021).
URL https://instrumentationjournal.com/index.php/instr/article/view/263/206

[7] A. Carrierou, C. Join, J.-P. Condomines, Restricted model control applied to the quanser aero with uncertain parameters, in: Proceedings of the $15^{th}$ Annual International Micro Air Vehicle Conference and Competition (IMAV 2024), Bristol, United Kingdom, 2024, pp. 270–276, paper no. IMAV2024-32.
URL https://www.imavs.org/papers/2024/32.pdf

[8] Q. Inc., Quanser AERO 2-DOF Lab Guide, laboratory documentation (2024).
URL https://users.encs.concordia.ca/~realtime/elec483/docs/Quanser%20AERO%20-%202DOF%20Lab%20Guide.pdf

[9] J. M. Portella Delgado, A. Goel, Adaptive nonlinear control of a bicopter with unknown dynamics, in: 2024 American Control Conference (ACC 2024), IEEE, 2024, pp. 3867–3872. doi:10.23919/ACC60939.2024.10644601.

[10] J. M. Portella Delgado, M. Mirtaba, A. Goel, Adaptive backstepping control of a bicopter in pure feedback form with dynamic extension, arXiv preprint arXiv:2402.03709 (2024).


## Appendix